ChemPubSoc Europe

DOI: 10.1002/chem.201700717

CHEMISTRY A European Journal Full Paper

Medicinal Chemistry |*Hot Paper*|

Exploring the Influence of the Aromaticity on the Anticancer and Antivascular Activities of Organoplatinum(II) Complexes

Ana Zamora,[a] Sergio A. Pérez,[a] Matthias Rothemund,[b] Venancio Rodríguez,[a] Rainer Schobert,[b] Christoph Janiak,[c] and José Ruiz*[a]

Abstract: A series of new organometallic Pt^{II} complexes of the type [Pt(C^N)Cl(DMSO)] (C^N = *N*,*N*-dimethyl-1-(2-aryl)-methanamine-κ^2*C2*,*N*; aryl = phenyl **2a**, biphenyl **2b**, *p*-terphenyl **2c**, naphthyl **2d**, anthracenyl **2e**, or pyrenyl **2f**) have been synthesized to explore the influence of the aromaticity on their anticancer activity. The best performers, **2b** and **d**, are more active than cisplatin (CDDP) in epithelial ovarian carcinoma cells A2780, with **2d** having a higher selectivity factor than CDDP in all the tested cell lines. In addition, all the new compounds overcome the acquired resistance in A2780cisR cells and interestingly, show low micromolar IC_{50} values towards the triple negative breast cancer cell line MDA-MB-231 and the highly metastatic 518A2 melanoma cells. This study shows that the hydrophobicity, accumulation into cells, and metal levels on nuclear DNA for the complexes are consistent with their cytotoxicity. Complexes **2b** and **d** induce apoptosis in a caspase-independent manner and suppress the intracellular ROS generation without modifying the mitochondria membrane potential. In addition, **2a**–**f** effectively inhibit angiogenesis in the endothelial cell line EA.hy926 at sub-cytotoxic concentrations and **2b** and **d** show in vivo antivascular effects on the chorioallantoic membrane (CAM) of fertilized SPF-eggs (SPF = specific-pathogen-free). Inhibition of tubulin polymerization and degeneration of cytoskeleton organization in 518A2 melanoma cells are presented as a preliminary mechanism of its anti-metastatic activity.

Introduction

Cisplatin (CDDP) and the following generations of platinum-based drugs have become established chemotherapeutics for applying to various types of cancers for the past 40 years.[1] However, their effectiveness is still hindered by clinical problems, including a limited spectrum of activity and high toxicity leading to side effects such as nephrotoxicity, ototoxicity, and neurotoxicity.[2] Indeed, their lack of activity is usually linked to the development of acquired or intrinsic resistance,[3] the mechanisms of which are related to their ADMET (absorption, distribution, metabolism, excretion and toxicity) properties.[4]

Platinum chemotherapy is mostly reported for the treatment of advanced tumors, which almost always present metastatic lesions. However, they are rarely active to tumor metastases so that clinical protocols are usually based on a combination of platinum compounds with antiangiogenic drugs, such as taxanes.[5] It is noteworthy how the reduction of metastasis pathways strengthens the activity of carboplatin against ovarian cancer.[6]

In this way, new approaches rely on the development of organometallic compounds with both anticancer and antiangiogenic properties.[7] The advantage of these multiple anticancer activities is that the risks of systemic toxicity caused by administration of more than one anticancer drug would be strongly decreased.[8] Although for most of the cited examples the mechanism by which these drugs inhibit angiogenesis remains elusive, proteins such as growth factors,[7h,9] tubulin,[7f,10] or enzyme cathepsin B[11] seem always to be involved. Even though proteins are considered as non-traditional targets for metal complexes, some reviews highlight the importance of the metallodrug–protein interaction.[12] They are starting to be considered in such a way that even a chemical proteomics approach has been developed to identify potential protein targets for ruthenium–arene complexes bearing the 1,3,5-triaza-7-phosphaadamantan ligand (RAPTA) agents.[13] Hydrophobic interactions with proteins can be promoted by increasing the hydrophobicity of the metallodrugs, which at a time is likely to result in higher drug accumulation into cells.[14] Therefore, physicochemical properties such as lipophilicity should be op-

[a] *A. Zamora, S. A. Pérez, Dr. V. Rodríguez, Prof. Dr. J. Ruiz*
Departamento de Química Inorgánica and
Regional Campus of International Excellence "Campus Mare Nostrum"
Universidad de Murcia, and Institute for Bio-Health
Research of Murcia (IMIB-Arrixaca), 30071 Murcia (Spain)
E-mail: jruiz@um.es

[b] *M. Rothemund, Prof. Dr. R. Schobert*
Organic Chemistry Laboratory, University Bayreuth
Universitaetsstrasse 30, 95440 Bayreuth (Germany)

[c] *Prof. Dr. C. Janiak*
Institut für Anorganische Chemie und Strukturchemie
Heinrich-Heine-Universität Düsseldorf
Universitätsstr. 1, 40225 Düsseldorf (Germany)

Supporting information and the ORCID identification number(s) for the author(s) of this article can be found under:
http://dx.doi.org/10.1002/chem.201700717.

timized through structural modifications in order to improve the likelihood of the drug success.[15] Adjusting this pharmacological parameter is a matter of great interest and its correlation with the antiproliferative activity of Pt^{IV}, Ru^{II}, Ir^{III} and Os^{II} metallodrugs has been studied. Some of the most used strategies include varying the arene ligand aromaticity in "piano-stool" complexes,[16] controlling the nature of axial ligands in octahedral Pt^{IV} complexes,[17] or changing the spacer length in dinuclear Ru^{II} complexes.[18] Indeed, the kinetically inert CN ligand, which also offers higher stability than most other bidentate ligands, has also been modified for this purpose by introducing diverse functionalities[7j,19] or lipophilic pendants such as estrogens.[20]

We have recently reported a series of compounds of the type [Pt(C^N)Cl(DMSO)] (C^N = *C,N*-dimethylbenzylamine-like ligand) with dual antiangiogenic and cytotoxic activities in vitro.[21] Since the dual activity is not strongly affected by the introduction of R-substituents into the *C,N*-chelating ligand, this scaffold offers the potential to fine tune the lipophilicity of the metallodrug. Thus, we have aimed herein to synthesize a series of *N,N*-dimethyl-1-(2-aryl)methanamines platinum(II) complexes (Scheme 1) to explore the impact of the aromaticity

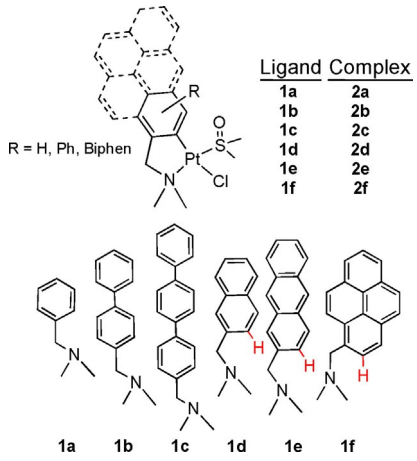

Scheme 1. Structures of the *C,N*-cycloplatinated *N,N*-dimethyl-1-(2-aryl)methanamines drugs. C–H bond-activation position is shown for ligands **1 d–f**.

on their anticancer activity against a panel of ovarian and breast cancer cells. Their activity has been related to the intracellular accumulation and the Pt-bound to nuclear DNA, as well as an additional mitochondrial dysfunction. We further study their efficacy to inhibit the angiogenesis in vitro, which afterwards was also checked in vivo with the chorioallantoic membrane (CAM) assay.

Results and Discussion

Synthesis and characterization of the dimethyl-1-(2-aryl)methanamine complexes 2 a–f

Ligands **1 b–f** were prepared by nucleophilic aromatic substitution[22] (**1 d**), reductive amination[23] (**1 b**, **e**, and **f**) of the appropriate aldehyde, or Suzuki–Miyaura cross-coupling (**1 c**). Cyclometalation of the *cis*-$PtCl_2(DMSO)_2$ with the corresponding dimethyl-1-(2-aryl)methanamine **1 a–f** in the presence of NaOAc affords the respective organoplatinum complexes **2 a–f** (Scheme 1).

The complexes were characterized by NMR spectroscopy, including ^1H, ^{13}C, ^{195}Pt, and two-dimensional techniques such as COSY, NOESY and HSQC (Figures S1–S6 in the Supporting Information) for the full assignment. The ^1H NMR spectra of all complexes show the presence of four resonances flanked by ^{195}Pt satellites; those assigned to the methyl groups of the DMSO ligand, the benzylic protons, and the NMe_2 of the donor arm, as well as a CH of the phenyl ring. This signal, assigned to H^6 (**2 a**, **b**, and **c**), H^1 (**2 d** and **e**) or H^{10} (**2 f**) with ($^3J_{H\text{-}Pt} \approx 50$ Hz), ensures the *C,N*-coordination of the deprotonated chelating ligands. In the case of ligand **1 d** and **e**, the cyclometalation position was easily recognized by the presence of two (**2 d**) or four (**2 e**) singlets in the ^1H NMR spectrum. However, in the case of **2 f**, complete assignment of the structure required confirmation by X-ray diffraction (vide infra). The result is in agreement with the fact that in the absence of a directing group, such as bromide or iodide,[24] the metal induces a certain degree of regioselectivity so that cyclometalation of ligand **1 d–f** occurs at the least sterically hindered position and yields exclusively the five-membered metallacycles **2 d–f**.

Based on NOESY experiments (Figure S4 in the Supporting Information for **2 d**), the expected DMSO *trans* to NMe_2 ligand arrangement was confirmed. A strong cross-peak was observed between H^1 and the methyl protons of DMSO, and another between H^6 and the CH_2 of the amine. The positive-ion ESI-MS displayed the peaks $[M-Cl]^+$ with the expected isotopic distribution pattern. All compounds were shown to be at least 95% pure by both elemental analyses and RP-HPLC.

Structure determination

Single crystals suitable for X-ray diffraction analysis were obtained from the slow diffusion of hexane into a saturated solution of **2 c** and **f** in CH_2Cl_2/toluene and CH_2Cl_2, respectively.

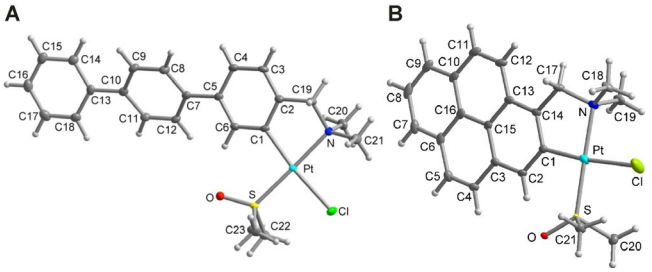

Figure 1. Molecular structures with atom numbering schemes for (A) **2 c** (50% thermal ellipsoids) and (B) **2 f** (50% thermal ellipsoids). Selected bond lengths (Å) and angles (°) for **2 c**: Pt–C1 = 2.016(2), Pt–N = 2.1102(19), Pt–S = 2.2107(6), Pt–Cl = 2.4022(6), C1–Pt–N = 81.12(9), N–Pt–Cl = 92.35(6), S–Pt–Cl = 88.95(2), C1–Pt–*S* = 97.64(7), N–Pt–S = 177.82(6), C1–Pt–Cl = 172.93(7). Selected bond lengths (Å) and angles (deg) for **2 f**: Pt–C1 = 2.008(3), Pt–N = 2.095(2), Pt–S = 2.1992(6), Pt–Cl = 2.4039(7), C1–Pt–N = 82.01(9), N–Pt–Cl = 91.69(6), S–Pt–Cl = 87.36(2), C1–Pt–*S* = 98.92(7), N–Pt–S = 178.90(6), C1–Pt–Cl = 173.20(7).

Their structures and atom numbering schemes are shown in Figure 1. Crystallographic data are shown in Tables S2 and S9 and bond lengths and angles are listed in Tables S7 and S14 in the Supporting Information. For both compounds **2c** and **f**, the Pt atom is in a distorted square planar environment, with the C–Pt–N bite angle deviating from 90° due to the bite of the cyclometalated ligand. As was suggested from NMR solution studies, the *S*-bonded DMSO ligand is positioned *trans* to the NMe_2 group, which automatically positions the chlorido ligand *trans* to the aryl ring of the *C,N*-chelate. The values of the Pt–C and Pt–N distances of the bonded deprotonated dimethyl-1-(2-aryl)methanamine ligand are within the normal ranges expected for such cyclometalated complexes.[25] In complex **2c** the dihedral angles between the terminal and central phenyl ring to the metal-bound phenyl ring are 7.31(6)° and 26.31(6)°, respectively (Figure S15). The packing in the structure of both complexes is organized by intermolecular C–H···O,[26] C–H···Cl,[27] C–H···π[28] and van der Waals interactions (Tables S8 and S15 and Figures S14 and S16). There are no significant π–π interactions.[29]

Biological activity

Complexes **2a–f** were evaluated in vitro for their antiproliferative activity using a MTT-based proliferation assay against a panel of human cancer and non-tumorigenic cell lines (Table 1). Due to their low solubility in aqueous solution, the tested compounds were first dissolved in DMSO and then serially diluted in complete culture medium such that the effective DMSO content did not exceed 0.4%. CDDP was used as positive control.

The dimethyl-1-(2-aryl)methanamine complexes **2a–f** showed distinct antiproliferative activity against the studied cancer cell lines with IC_{50} values in the low micromolar range. All of them displayed the highest activity in the A2780 epithelial ovarian cell line, against which the complexes containing two aromatic rings—biphenyl (**2b**) and naphthyl (**2d**)—were the best performers. Aside from being more active than CDDP in both ovarian A2780 and A2780cisR cancer cells, all of the complexes were also able to overcome the acquired resistance that A2780cisR develops to CDDP, with a resistance factor (RF) below 2.[30]

On the other hand, an anticancer activity reduction towards the multidrug resistant MCF-7 and the triple negative MDA-MB-231 breast carcinoma cells respect to ovarian cancer cells was observed. Interestingly, it is worth noting that **2a–f** proved markedly more cytotoxic than CDDP (>20 μM) in the highly metastasic MDA-MB-231 cells. In addition, this reduction in activity was observed in the also highly metastatic 518A2 melanoma cells. Notably, **2b** and **d** are more active than the rest of the series with IC_{50} in the same order of magnitude as CDDP.

Moreover, the in vitro antiproliferative activity was also evaluated against non-tumorigenic renal BGM cells to determine their differential selectivity towards cancer versus normal cells. All the complexes were found to be less toxic than CDDP and more importantly, selectivity factor values (SF = BGM cells IC_{50} divided by cancer cells IC_{50}) attest to a preferential cytotoxicity of Pt^{II} organometallic complexes towards neoplastic cells with SF values ranged from 1.06–10× higher than CDDP (Figure S9 in the Supporting Information). Overall, the complex **2d** is the best performer because it meets the requirements of being one of the most potent agents with the higher SF values in all the tested cancer cell lines. This result might contribute to increase the likelihood of tumor specificity of these anticancer drugs. The value of this experiment is meaningful with respect to the nephrotoxicity frequently observed for other metal-based chemotherapeutics.

On the other hand, IC_{50} values for **2a–f** in the immortalized endothelial EA.hy926 cell line were also calculated with the aim to verify that the antiangiogenic effect was not due to a cytotoxic effect but rather to their antiangiogenic potential.

Apoptosis studies

To assess whether the complexes cause cell death by apoptosis or necrosis, Annexin V (AV)/Propidium iodide (PI) dual-staining assay was performed in A2780 cells after 48 h incubation of **2b** and **d** at 1 μM.

The results in Figure 2 are depicted in diagrams showing the four typical quadrants, which distinguish between viable cells

Table 1. IC_{50} values (μM) for **2a–f** and CDDP at 48 h. Resistance Factors are given in parentheses.

Complex	A2780[a]	A2780 cisR[b] (RF)	MCF-7[c]	MDA-MB-231[d]	518A2[e]	BGM[f]	EA.hy926[g]
2a	1.38 ± 0.37	2.05 ± 0.24 (1.49)	>20	7.33 ± 2.34	8.30 ± 0.36	7.87 ± 2.22	14.09 ± 4.91
2b	1.18 ± 0.10	1.51 ± 0.34 (1.29)	10.67 ± 0.06	4.36 ± 0.67	3.73 ± 0.69	3.56 ± 0.54	3.70 ± 0.98
2c	2.08 ± 0.16	2.61 ± 0.39 (1.25)	10.30 ± 1.04	5.14 ± 1.22	7.07 ± 0.33	5.58 ± 1.20	5.23 ± 0.16
2d	1.29 ± 0.09	1.97 ± 0.24 (1.53)	13.79 ± 2.38	6.00 ± 1.56	5.41 ± 0.20	7.33 ± 2.64	5.92 ± 1.17
2e	2.10 ± 0.08	2.34 ± 0.39 (1.12)	16.07 ± 1.68	5.41 ± 0.49	7.06 ± 0.06	6.56 ± 1.91	5.95 ± 0.15
2f	2.04 ± 0.25	2.38 ± 0.18 (1.16)	9.46 ± 0.55	5.13 ± 2.13	9.21 ± 0.29	4.84 ± 1.99	4.51 ± 1.42
CDDP	1.63 ± 0.35	24.13 ± 2.88 (14.80)	>20	>20	2.72 ± 0.23	3.47 ± 0.65	11.08 ± 2.71

[a] **A2780**: human sensitive ovarian cancer cells; [b] **A2780 cisR**: human CDDP-resistant ovarian cancer cells; [c] **MCF-7**: human breast cancer cells (ER+, PR+, ER = estrogen receptor, PR = progesterone receptor, +/− indicates receptor status, present or absent); [d] **MDA-MB-231**: triple negative human breast cancer cells (ER−, PR−, no HER2 overexpression, HER2 = human epidermal growth factor 2); [e] **518A2**: human melanoma cells; [f] **BGM**: normal African green monkey kidney cancer cells; [g] **EA.hy926**: immortalized endothelial cells.

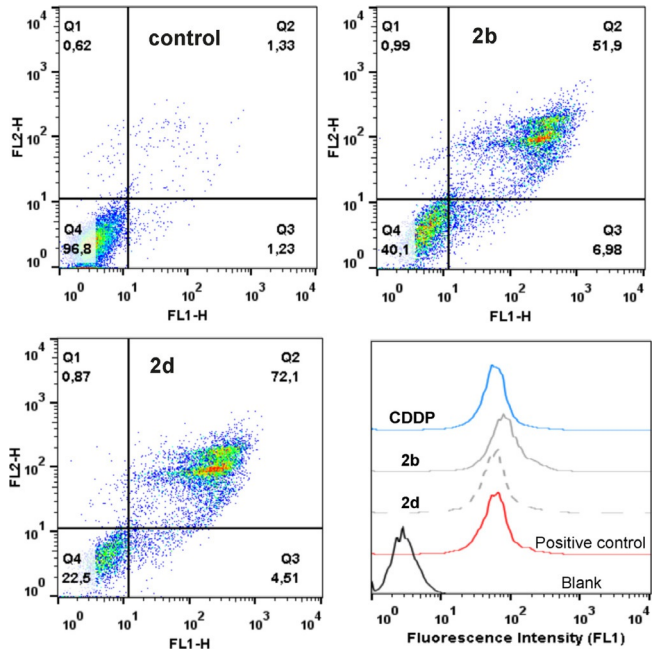

Figure 2. Flow cytometry analysis of A2780 cells after 48 h treatment with 1 μM of **2b** and **d** as detected by annexin V/PI. Caspase-3 activation (lower right) in A2780 cells caused by 24 h exposure to 1 μM of **2b** and **d**. Blank are cells without dye and positive control are cells treated with the dye.

(Q4, AV−/PI−), early apoptosis (Q3, AV+/PI−), late apoptosis (Q2, AV+/PI+), and necrosis (Q1, AV−/PI+). As can be seen clearly, **2b** and **d** induce a high incidence of apoptosis (58.9% and 76.6%, respectively) in A2780 cells at 48 h without increasing the necrotic population (<1%). This result is consistent with previous studies[21] that showed an increase in Annexin V-positive apoptotic cells with the exposure time to related compounds.

To clarify the mechanism by which the complexes induce apoptosis, the activity of caspase-3 was examined using the caspase-3 detection kit (FITC-DEVD-FMK) in A2780 cells after 24 h exposure to 1 μM of **2b** and **d**. Caspase-3 is one of the key executers of apoptosis, responsible for the proteolytic cleavage of key protein such as the poly(ADP-ribose) polymerase (PARP).[31] As shown in Figure 2, no enhancement of caspase-3 activity was found after **2b** or **d** exposure with respect to the positive control. Therefore, these complexes may promote a caspase-independent cell death with mitochondria playing the central role (vide infra).

Hydrophobicity, cellular platinum accumulation and cytotoxicity relationship

The effect of the *C,N*-chelate on the drug lipophilicity was studied by comparison of their RP-HPLC retention times (t_R) on a C18 column. This is considered a reliable method to estimate the relative hydrophobicities, since the RP-HPLC behavior of a compound depends on its hydrophobic interactions with the non-polar stationary phase: the more hydrophobic a compound is, the higher its t_R is.[17a,32] As expected, all the synthesized analogues of **2a** were found to be more lipophilic

Table 2. Retention times (t_R) by RP-HPLC, platinum cellular accumulation (at 10 μM) in A2780 cells treated for 3 h for **2a–f** and CDDP.

Complex	t_R (min)	Accumulation [ng Pt/10^6 cells]	ng Pt/μg DNA
2a	7.44±0.04	7.72±0.33	10.15±0.31
2b	9.12±0.18	12.10±1.03	16.00±0.22
2c	10.78±0.50	1.26±0.10	3.41±0.07
2d	8.54±0.10	10.81±0.54	14.04±0.65
2e	10.04±0.13	2.47±0.18	4.38±0.04
2f	9.97±0.42	2.18±0.11	0.022±0.001
CDDP	–	0.49±0.06	0.107±0.002

(Table 2). In general, hydrophobicity plays an important role in the ability of organometallic complexes to accumulate into cells and as a result, their antitumor activity increases.[16d,17–20,33] Therefore, cellular platinum accumulation in A2780 cells after 3 h exposure to **2a–f** (10 μM) was determined by inductively coupled plasma mass spectrometry (ICP-MS, Table 2).

The results show a correlation between hydrophobicity and accumulation for the most active compounds **2b** and **d** with respect to the parent **2a**, as well as between their accumulation and anticancer activity (Figure S10 in the Supporting Information). However, it is to be noted that this trend is not so observable when the hydrophobicity is higher than that of the derivative **2b**. So, the level of platinum accumulation for the most lipophilic derivatives **2c**, **e**, and **f** was found to be drastically lower than that of **2a**, which correlates with the reduction in anticancer activity found. This reduction of both accumulation and potency for **2c**, **e**, and **f** with respect to **2a** may be attributed to their high hydrophobicity, which seems to be outside the optimal range. In fact, high hydrophobicity values also designated as "molecular obesity" are often linked to the lack of adequate pharmacokinetic profiles, finally compromising their in vitro potency.[15,34]

Cellular localization and distribution

Taking advantage of the inherently fluorescent pyrenyl ring of complex **2f**, its intracellular distribution was investigated in living cultured MCF-7 cells by confocal microscopy. Cells were incubated for 1 h with **2f** at 1 μM and both nuclei and mitochondria were stained with 500 nM SYTO® and 200 nM Mitotracker for 30 min, respectively. Multispectral imaging fluorescence microscopy was used to simultaneously acquire high-resolution images (Figure 3 and Figure S11 in the Supporting Information).[35]

The **2f** images did not significantly differ from the mitochondria-labelled ones whereas negligible nuclear uptake was observed after 1 h incubation. Although unexpected, **2f** appeared to be mainly localized in the cytoplasm. Since the compounds were designed to act as monofunctional anticancer agents,[21,36] and some examples have been recently reported of metallodrugs for which fluorescence microscopy suggested perinuclear and cytosolic uptake, but quantification by ICP-MS clearly evidenced a major uptake into the nucleus,[37] metal levels on nuclear DNA were determined in A2780 cells after

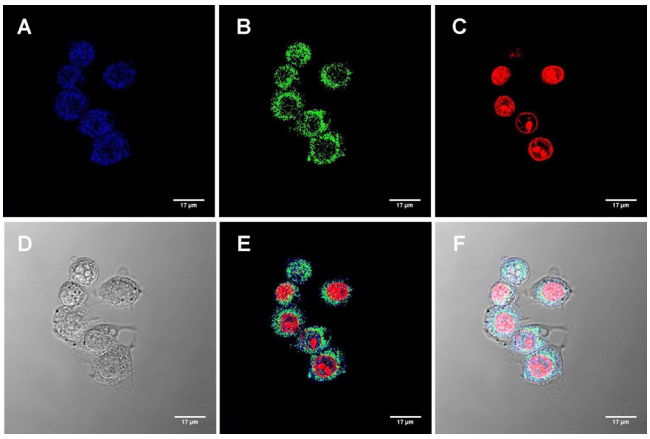

Figure 3. Confocal imaging of MCF-7 cells treated with conjugate **2f** for 1 h (A), Mitotracker® FM green (B) and SYTO® 59 Red (C) for 30 min. Phase contrast (D) and A-C merged image (E) and A–D merged image (F). Blue fluorescence (λ_{ex} = 458 nm, λ_{em} = 458–472 nm) represents compound **2f**, green fluorescence (λ_{ex} = 488 nm, λ_{em} = 516–538 nm) represents mitochondria of MCF-7 cells and red fluorescence (λ_{ex} = 633 nm, λ_{em} = 636–675 nm) represents nuclei of MCF-7 cells. Scale bars = 17 μm.

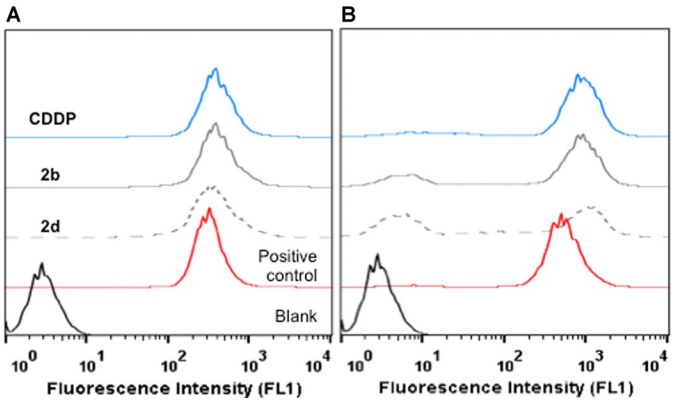

Figure 4. Flow cytometry analysis of (A) mitochondrial membrane potential and (B) ROS generation in A2780 cells after 24 h treatment with 1 μM of **2b**, **d**, or CDDP. Blank are cells without dye and positive control are cells treated with the corresponding dye.

3 h exposure to 10 μM of the compounds. The data in Table 2 show that the amount of platinum associated to nuclear DNA was higher for the most active derivatives. Similarly to the results of platinum accumulation, a reduction is observed for **2c** and **e**, becoming almost negligible for **2f**, in agreement with the confocal microscopy study in MCF-7 cells. Therefore, the reduction in activity of **2c**, **e**, and **f**, may be explained as a result of their lack of DNA interaction. Moreover, their DNA-binding behavior was assessed using an electrophoretic mobility shift assay (EMSA). Dose responses were performed for **2b** and **d** with circular pBR322 plasmid DNA at 37 °C for 24 h (Figure S12 in the Supporting Information). **2b** slightly reduced the mobility of plasmid DNA at low concentration (10 μM) and produced the smearing of the band at higher concentration (50 μM). In contrast, **2d** showed a lesser extent of interaction with the DNA. In conclusion, the covalent interaction with DNA via monoadduct formation, as previously reported for this type of complexes,[21] cannot be diminished. Likewise, the weak fluorescence signal in the nucleus may be explained assuming that a short period of time such as 1–3 h was not enough for the hydrophobic **2f** derivative to accumulate into the nucleus.

To gain more insight into a possible mitochondria-destabilizing activity of the compounds, the mitochondrial membrane potential and the intracellular reactive oxygen species (ROS) production was studied by flow cytometry (Figure 4).

For this purpose, Rhodamine-123 (Rho-123) and 2′,7′-dichlorodihydrofluorescein diacetate (DCFH-DA) were used to measure the effect in A2780 cells after treatment with **2b** and **d** (1 μM) for 24 h. As shown in Figure 4, the addition of the compounds does not produce a distinguishable variation in the fluorescence of Rho-123, indicating no changes in the mitochondrial membrane potential. On the other hand, a 26.20% for **2b** and 41.9% for **2d** fluorescence reduction of the DCF oxidation product was observed, which indicates a capability of both complexes to suppress the mitochondrial ROS generation. Although the majority of the metallodrugs that disrupt the mitochondrial function involve oxidative stress,[38] some examples of ROS inhibition have been reported.[39] In fact, one approach to enhanced cell cytotoxicity relies on the combination of ROS-generating and ROS-scavenging agents.[40] This mitochondrial activity of the compounds may be related with the death of cancer cells independently of the classical caspase cascade. Indeed, the abolition of mitochondrial ROS generation could be also linked to their inhibition of in vitro angiogenesis tube formation (vide infra).[41]

In vitro and in vivo antivascular activity

We previously showed that introduction of R-substituents to the negatively charged *C,N*-chelated dimethylbenzylamine ligands slightly affect the dual antitumor and antiangiogenic activity of the corresponding organoplatinum complexes.[21] We now studied if the lipophilicity of related organometallic Pt^{II} complexes might adjust their antiangiogenic potential as well.

Considering that endothelial cell proliferation is essential in the multistep process of angiogenesis, in vitro vascular tube formation assay was measured 12 h after incubating EA.hy926 cells with **2a**–**f** at 1 μM, that is, at sub-cytotoxic concentrations. CDDP was used at equimolar concentrations for comparative purposes. The results of the two-dimensional Matrigel assay were quantified (Figure 5A) by calculating the total length (μm), number of meshes (network or polygonal structures), and total meshes area (area occupied by the meshes, μm^2). Complexes **2a**–**f** effectively inhibit the formation of capillary-like structures at sub-cytotoxic concentrations, since only fragmented tubules and some sprouting points could be distinguished (Figure 5B). Interestingly, an enhancement of lipophilicity resulted in a higher inhibitory effect with respect to the **2a** parent compound. In addition, **2b** and **d** stand out for their antiangiogenic, as well as their antitumor activities.

Further studies were carried out to examine the in vivo antivascular effects of **2b** and **d** by using the chick embryo's chorioallantoic membrane (CAM) assay as a model system.[42]

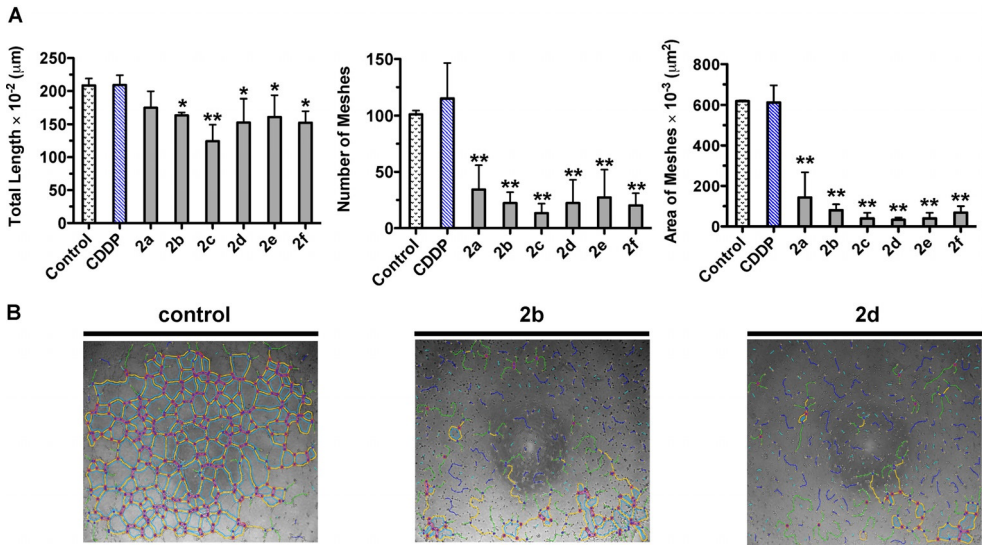

Figure 5. Effect of complexes **2a**–**f** in the endothelial cell tube formation assay. (A) Quantification after the ImageJ process of number of meshes, total meshes area, and total length of tubular structure of EA.hy926 cells under 1 μM of compounds and CDDP for 12 h. Error bars indicate ± standard deviations for two sets of three data points for each compound. $*p<0.05$ and $**p<0.01$ was considered to be statistically significant. (B) Typical images after ImageJ process of EA.hy926 cells added to 96-well plates precoated with Matrigel for 12 h: for culture medium as a control **2b** and **d**. Tube formation of EA.hy926 cells was photographed under an inverted phase-contrast microscope.

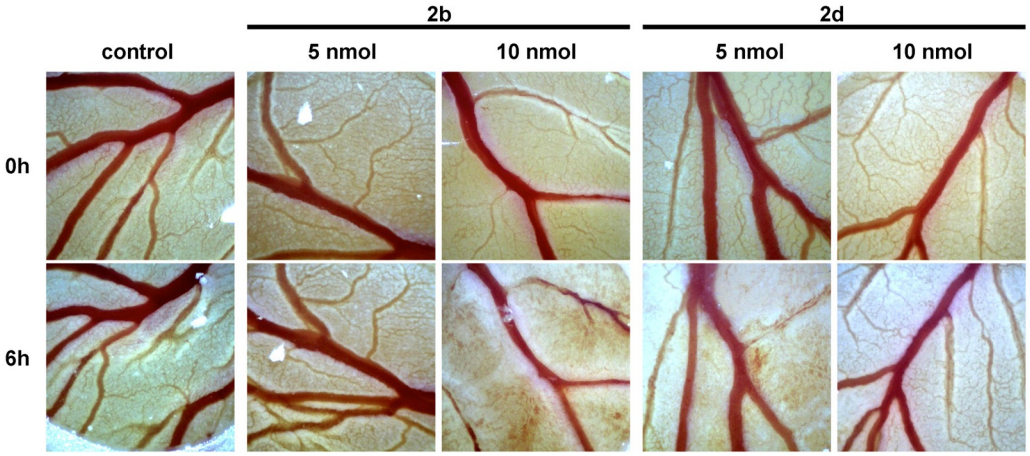

Figure 6. Effects of treatment with 5 or 10 nmol of **2b** and **d** on the CAM of fertilized SPF-Eggs after 6 h. Control contains an equal amount of DMSO; images are representative of three independent experiments. Magnification 60×.

Figure 6 shows the effect of 6 h treatment with **2b** and **d** at 5 and 10 nmol in comparison with the control, treated with equivalent amounts of DMSO. Both complexes showed antivascular effects on the blood vessels in the CAM of fertilized chicken eggs, whereas no changes could be observed during incubation with DMSO. **2b** showed significant vascular-disruptive effects even degrading big blood vessels at 10 nmol and interestingly, **2d** showed a much stronger effect at 5 nmol than 10 nmol, in which almost all the small capillaries disappeared and bigger vessels were starting to degrade.

Microtubules: tubulin staining and microtubule polymerization inhibition

Tumor vasculature can be addressed by angiogenesis-inhibiting agents that target vascular endothelial growth factor (VEGF) and its receptor (VEGFR) or other pro-angiogenic pathways, as well as vascular-disrupting agents, which have shown an apoptotic effect or affect the cytoskeleton.[43] Considering that the compounds have shown synergism of cytotoxic effect and damage tumor blood vessels in vivo, we investigated the effects of **2b** and **d** on the tubulin polymerization and microtubule organization.

The fluorescence-based tubulin polymerization assay (Figure S13 in the Supporting Information) shows how **2b** and to a lesser extent **2d** inhibited the polymerization of tubulin at 20 μM, in comparison to the control and combretastatin A-4 (CA-4), a known inhibitor of microtubule formation.[44]

After that, the effect of both complexes on the cytoskeleton organization of microtubules was studied in 518A2 melanoma cells (Figure 7).

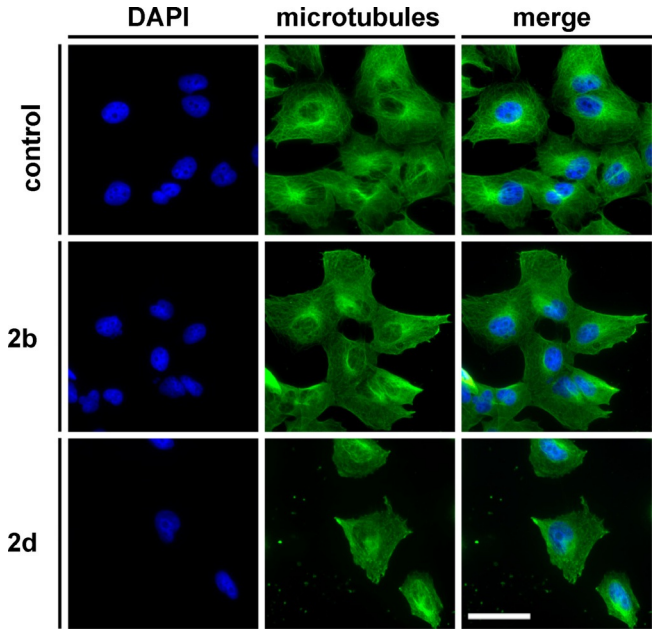

Figure 7. Effects on the cellular organization of microfilaments. Fluorescence microscopy visualization of microtubules (anti-alpha-tubulin) and nuclei (DAPI) in 518A2 melanoma cells after 24 h incubation with DMSO (control) or 2 μM of **2b** and **d**. 400-fold magnification, scale bar: 50 μm; images are representative of two independent experiments.

Typical tubulin polymerization inhibitors such as CA-4 cause, through direct interaction with tubulin, the destabilization and eventually disintegration of the tubulin cytoskeleton and resulting to disintegration of cellular organization. In endothelial cells, this effect causes the degradation of formed (tumor) blood vessels.[44] As expected, a normal distribution of microtubules throughout the cells was observed for untreated control cells (containing an equivalent amount of DMSO used for the compounds). However, 24 h incubation with 2 μM of **2d** shows an almost completely degenerated tubulin network, not only the number was reduced, but the cells also appeared rounded in comparison to the control or cells treated with 2 μM of **2b**. In contrast, treatment of melanoma cells with 2 μM of **2b** resulted in a slight change in the tubulin network; the microtubules maintained a defined structure although a starting degradation of the tubulin network is noticeable around the nuclei.

Conclusion

We have explored the influence of the aromaticity on the anticancer and antivascular activities of a series of new Pt^{II} compounds [Pt(C^N)Cl(DMSO)] **2a–f** based on *N,N*-dimethyl-1-(2-aryl)methanamines as the C^N backbone. They exhibited IC_{50} values in the low micromolar range towards human ovarian, breast cancer and melanoma cell lines, resulting markedly more cytotoxic than CDDP in the metastatic MDA-MB-231. This study shows how the hydrophobicity increment from **2a** to **2b** and **d** resulted in a higher accumulation into cells, which explains their higher anticancer activity. However, when further structural changes are carried out from **2a** to **2c**, **e**, and **f**, no correlation between hydrophobicity and accumulation was found and consequently their anticancer activity drops below that of the parent **2a.** This suggests that there is an optimal range for the extension of aromaticity/lipophilicity in this type of compounds. In mechanism studies, **2b** and **d** were shown to activate apoptotic cascades, to decrease the production of ROS in A2780 cells without modifying the mitochondria membrane potential, and interact with DNA. In addition, their anti-angiogenesis effects along with their capability to inhibit tubulin polymerization and degenerate the cytoskeleton network provide evidence that the complexes act as vascular disrupting agents, which was checked in vivo for **2b** and **d** in the CAM assay.

Experimental Section

General methods

All synthetic manipulations were carried out under an atmosphere of dry, oxygen-free nitrogen using standard Schlenk techniques. Solvents were dried by the usual methods. The compounds *cis*-$[Pt(DMSO)_2Cl_2]$[45] and **2a**[46] were prepared following published procedures. All other reagents were obtained from commercial sources and used without further purification.

The C, H, N, and S analyses were performed with a Carlo Erba model EA 1108 microanalyzer. The ^{1}H, ^{13}C, and ^{195}Pt NMR spectra were recorded on either a Bruker AC 300E or a Bruker AV 400 spectrometer. Chemical shifts are cited relative to $SiMe_4$ (^{1}H and ^{13}C, external) and $Na_2[PtCl_6]$ (^{195}Pt, external). ESI-MS, compound purity, and stability analyses were performed on a HPLC/MS TOF 6220. Chromatographic analyses were carried out on a Brisa C18 column (150 mm × 4.6 mm, 5 μm particle size). The isotopic distribution of the heaviest set of peaks matched very closely that calculated for the formulation of the complex cation in every case.

Synthesis of anthracene-2-carbaldehyde

2-Bromoanthracene (1.0 g, 3.89 mmol) was dissolved in dry THF (60 mL) under N_2 atmosphere. A solution of *n*BuLi (4.8 mL, 1.6 M in hexane, 7.78 mmol) was added dropwise to the reaction mixture at −70 °C to afford a dark red solution upon warming to −15 °C. The reaction mixture was cooled to −70 °C and an excess of DMF (5 mL) was added. As mixture warmed to 0 °C, it turned into a yellow solution, which was poured into ice under vigorous stirring. It was allowed to reach RT overnight. The organic solvents were removed in vacuo, the precipitated filtered off, washed with water, and purified by column chromatography using AcOEt/hexane (10:90).

Yellow solid; Yield: 78%; ^{1}H NMR (400 MHz, $CDCl_3$): $\delta = 10.17$ (s, 1H, CHO), 8.60 (s, 1H, ArH), 8.48 (s, 1H, ArH), 8.45 (s, 1H, ArH), 8.07–8.03 (m, 3H, ArH), 7.90 (dd, 1H, ArH, $J_{HH} = 1.6$ Hz, $J_{HH} = 8.8$ Hz), 7.60–7.54 (m, 2H, ArH).

Synthesis of 1-([1,1′-biphenyl]-4-yl)-*N,N*-dimethylmethanamine (1b), 1-(anthracen-2-yl)-*N,N*-dimethylmethanamine (1e) and *N,N*-dimethyl-1-(pyren-1-yl)methanamine (1f)

Methanamines **1b, e**, and **f** were prepared by reductive alkylations of dimethylamine using the combination of titanium(IV) isopropoxide and sodium borohydride.[23a,b]

1b: Yellow oil that becomes solid upon storage; Yield: 74%. ^{1}H NMR (300 MHz, $CDCl_3$): δ = 7.62–7.55 (m, 4H, ArH), 7.47–7.31 (m, 5H, ArH), 3.48 (s, 2H, CH_2N), 2.29 (s, 6H, $N(CH_3)_2$); $^{13}C\{^1H\}$ NMR (75.46 MHz, $CDCl_3$): δ = 140.24, 138.00, 129.76, 128.95, 127.38, 127.27, 127.22, 64.23, 45.59.

1e: Orange solid; Yield: 72%; ^{1}H NMR (300 MHz, $CDCl_3$): δ = 8.39 (d, 2H, ArH, J_{HH} = 6.3 Hz), 8.01–7.96 (m, 3H, ArH), 7.86 (s, 1H, ArH), 7.50–7.44 (m, 3H, ArH), 3.63 (s, 2H, CH_2N), 2.33 (s, 6H, $N(CH_3)_2$); $^{13}C\{^1H\}$ NMR (75.46 MHz, $CDCl_3$): δ 136.01, 132.03, 131.81, 131.77, 131.38, 128.51, 128.38, 128.31, 127.62, 127.32, 126.19, 126.14, 125.54, 125.43, 64.88, 45.69.

1f: Yellow oil that becomes solid upon storage; Yield: 85%: ^{1}H NMR (300 MHz, $CDCl_3$): δ = 8.52 (d, 1H, ArH, J_{HH} = 9.3 Hz), 8.22–8.13 (m, 4H, ArH), 8.06 (s, 2H, ArH), 8.04–7.96 (m, 2H, ArH), 4.10 (s, 2H, CH_2N), 2.39 (s, 6H, $N(CH_3)_2$); $^{13}C\{^1H\}$ NMR (75.46 MHz, $CDCl_3$): δ = 132.83, 131.44, 131.06, 130.96, 130.07, 128.37, 127.59, 127.27, 125.98, 125.20, 124.98, 124.51, 124.06, 62.69, 45.88.

Synthesis of 1-([1,1′:4′,1″-terphenyl]-4-yl)-*N*,*N*-dimethylmethanamine (1c)

Ligand **1c** was synthesized using an adaptation method of reference [47].

Toluene (25 mL), methanol (15 mL), and water (0.30 mL) were added to biphenyl 4-boronic acid (1.0 g, 5.05 mmol), (4-bromobenzyl)dimethylamine (1.08 g, 5.05 mmol), tetrakis(triphenylphosphine)palladium (0.47 g, 0.40 mmol) and potassium carbonate (2.09 g, 15.20 mmol). The resulting mixture was heated at 80 °C overnight (16 h). The reaction mixture was then concentrated under reduced pressure, redissolved in hot chloroform and then filtered through a plug of Celite. The crude product was recrystallized from chloroform to give the desired terphenyl derivative.

White solid; Yield: 52%; ^{1}H NMR (300 MHz, $CDCl_3$): δ = 7.68 (s, 4H, ArH), 7.67–7.60 (m, 4H, ArH), 7.49–7.44 (m, 2H, ArH), 7.41–7.36 (m, 3H, ArH), 3.48 (s, 2H, CH_2N), 2.29 (s, 6H, $N(CH_3)_2$); $^{13}C\{^1H\}$ NMR (75.46 MHz, $CDCl_3$): δ = 139.99, 139.86, 139.42, 129.57, 128.79, 127.46, 127.37, 127.30, 127.02, 126.86, 64.05, 45.42.

Synthesis of *N*,*N*-dimethyl-1-(naphthalene-2-yl)methanamine (1d)

To a solution of dimethylamine (9.04 mmol, 1.6 mL) in DCM (20 mL) was added dropwise a solution of 2-(bromomethyl)naphthalene (2.26 mmol, 500 mg) in DCM (20 mL) under a N_2 atmosphere. The resulting solution was stirred overnight at RT and finally extracted with NaOH 5% (50 mL), water (50 mL), and brine (50 mL). The combined organic phases were dried with $MgSO_4$. The oil was purified by column chromatography using AcOEt/hexane (10:90) as eluent.

Yellow oil; Yield: 84%; ^{1}H NMR (300 MHz, $CDCl_3$): δ = 7.85–7.81 (m, 3H, ArH), 7.75 (s, 1H, ArH), 7.51–7.43 (m, 3H, ArH), 3.61 (s, 2H, CH_2N), 2.31 (s, 6H, $N(CH_3)_2$); $^{13}C\{^1H\}$ NMR (75.46 MHz, $CDCl_3$): δ = 136.39, 133.53, 132.97, 128.16, 127.93, 127.83, 127.54, 126.14, 125.81, 64.65, 45.57.

General Procedure for the Synthesis of Cycloplatinated Pt^{II} Complexes 2b–f

The method was adapted as previously described.[21] The corresponding amine (0.71 mmol) dissolved in MeOH (2 mL) was added under N_2 to a suspension of *cis*-$[PtCl_2(DMSO)_2]$ (0.71 mmol) and NaOAc (1.4 mmol) in 15 mL of freshly distilled MeOH. The resulting mixture was stirred at 65 °C and the reaction time was monitored by TLC. Cyclometalation of the amines completed at approximately 5–7 h for **1b** and **c**, and 24 h for **1d–f**. When the reaction finished, the solution was concentrated under vacuum and a white or pale yellow solid precipitated. The solid was filtered, washed with MeOH/ether, and air-dried. If required, column chromatography was carried out on silica gel using CH_2Cl_2/MeOH (95:5) as eluent.

2b: White solid; Yield: 72%; ^{1}H NMR (300 MHz, $CDCl_3$): δ = 8.28 (d, 1H, H^6, J_{HH} = 1.8 Hz, J_{HPt} = 49.5 Hz), 7.65–7.62 (m, 2H, CH of Ph), 7.43–7.28 (m, 4H, H^4 + CH of Ph), 7.13 (d, 1H, H^3, J_{HH} = 7.8 Hz), 4.04 (s, 2H, CH_2N, J_{HPt} = 39.9 Hz), 3.56 (s, 6H, SCH_3, J_{HPt} = 24.6 Hz), 2.96 (s, 6H, $N(CH_3)_2$, J_{HPt} = 33.6 Hz); $^{13}C\{^1H\}$ NMR (75.46 MHz, $CDCl_3$): δ 145.44 (s, Q), 141.83 (s, Q), 139.01 (s, Q), 136.42 (s, Q), 133.16 (s, CH^6, J_{CPt} = 56.0 Hz), 128.85 (s, CH), 127.34 (s, CH), 127.02 (s, CH), 123.83 (s, CH), 122.05 (s, CH^3, J_{CPt} = 36.8 Hz), 74.85 (s, CH_2N, J_{CPt} = 55.8 Hz), 52.51 (s, $N(CH_3)_2$), 47.01 (s, SCH_3, J_{CPt} = 63.1 Hz); ^{195}Pt NMR (86.18 MHz, $CDCl_3$): δ = −3657.55 (s); HRMS (ESI, pos. ion mode, CH_2Cl_2): *m/z* 483.1070 ($[M-Cl]^+$, calcd 483.1071); elemental analysis calcd (%) for $C_{17}H_{22}ClNOPtS$: C, 39.34; H, 4.27; N, 2.70; S, 6.18; found: C, 39.55; H, 4.16; N, 2.82; S, 6.25.

2c: White solid; Yield: 51%; ^{1}H NMR (300 MHz, $CDCl_3$): δ = 8.34 (d, 1H, H^6, J_{HH} = 1.8 Hz, J_{HPt} = 48.0 Hz), 7.74–7.69 (m, 2H), 7.67–7.61 (m, 4H), 7.47–7.31 (m, 4H), 7.15 (d, 1H, H^3, J_{HH} = 7.8 Hz, Pt satellites are observed as shoulders), 4.05 (s, 2H, CH_2N, J_{HPt} = 39.3 Hz), 3.57 (s, 6H, SCH_3, J_{HPt} = 23.7 Hz), 2.97 (s, 6H, $N(CH_3)_2$, J_{HPt} = 33.3 Hz); $^{13}C\{^1H\}$ NMR (75.46 MHz, $CDCl_3$): δ = 145.57 (s, Q), 141.15 (s, Q), 140.79 (s, Q), 139.83 (s, Q), 138.47 (s, Q), 136.47 (s, Q), 133.06 (s, CH^6), 128.97 (s, CH), 127.66 (s, CH), 127.62 (s, CH), 127.36 (s, CH), 127.23 (s, CH), 123.71 (s, CH), 122.11 (s, CH^3), 74.85 (s, CH_2N), 52.52 (s, $N(CH_3)_2$), 47.01 (s, SCH_3, J_{CPt} = 61.8 Hz); ^{195}Pt NMR (86.18 MHz, $CDCl_3$): δ = −3657.92 (s); HRMS (ESI, pos. ion mode, CH_2Cl_2): *m/z* 559.1388 ($[M-Cl]^+$, calcd 559.1385); elemental analysis calcd for $C_{23}H_{26}ClNOPtS$: C, 46.42; H, 4.40; N, 2.35; S, 5.39; found: C, 46.48; H, 4.52; N, 2.39; S, 5.39

2d: Pale yellow solid; Yield: 76%; ^{1}H NMR (400 MHz, $CDCl_3$): δ = 8.41 (s, 1H, H^1, J_{HPt} = 51.2 Hz), 7.82 (m, 1H, H^8), 7.67 (m, 1H, H^5), 7.54 (s, 1H, H^4), 7.37 (m, 2H, H^6 + H^7), 4.13 (s, 2H, CH_2N, J_{HPt} = 40.5 Hz), 3.59 (s, 6H, SCH_3, J_{HPt} = 23.2 Hz), 2.94 (s, 6H, $N(CH_3)_2$, J_{HPt} = 32.8 Hz);$^{13}C\{^1H\}$ NMR (150.9 MHz, $CDCl_3$): δ = 144.69 (s, Q), 133.58 (s, Q), 133.07 (s, CH^1, J_{CPt} = 78.8 Hz), 132.92 (s, Q), 131.71 (s, Q), 128.25 (s, CH^8), 126.99 (s, CH^5), 125.46 (s, CH^6 or CH^7), 125.15 (s, CH^6 or CH^7), 119.93 (s, CH^4, J_{CPt} = 39.8 Hz), 74.71 (s, CH_2N, J_{CPt} = 72.3 Hz), 52.35 (s, $N(CH_3)_2$), 47.04 (s, SCH_3, J_{CPt} = 95.1 Hz); ^{195}Pt NMR (86.18 MHz, $CDCl_3$): δ = −3663.46 (s). HRMS (ESI, (pos. ion mode, CH_2Cl_2): *m/z* 457.0910 ($[M-Cl]^+$, calcd 457.0915); elemental analysis calcd for $C_{15}H_{20}ClNOPtS$: C, 36.55; H, 4.09; N, 2.84; S, 6.51; found: C, 36.85; H, 4.15; N, 2.90; S, 6.40.

2e: Pale yellow solid; Yield: 70%; ^{1}H NMR (300 MHz, $CDCl_3$): δ = 8.57 (s, 1H, H^1, J_{HPt} = 53.7 Hz), 8.39 (s, 1H, H^5), 8.24 (s, 1H, H^{10}), 7.98–7.92 (m, 2H, H^6 + H^9), 7.70 (s, 1H, H^4), 7.44–7.37 (m, 2H, H^7 + H^8), 4.15 (s, 2H, CH_2N, J_{HPt} = 44.1 Hz), 3.62 (s, 6H, SCH_3, J_{HPt} = 32.4 Hz), 2.97 (s, 6H, $N(CH_3)_2$, J_{HPt} = 33.9 Hz); $^{13}C\{^1H\}$ NMR (75.46 MHz, $CDCl_3$): δ = 144.63 (s, Q), 133.15 (s, Q), 132.83 (s, CH^1), 131.82 (s, Q), 131.53 (s, Q), 131.45 (s, Q), 130.47 (s, Q), 128.56 (s, CH^6 or CH^9), 128.11 (s, CH^6 or CH^9), 126.22 (s, CH^5), 125.05 (s, CH^7 + CH^8 + CH^{10}), 119.70 (s, CH^4), 74.56 (s, CH_2N, J_{CPt} = 48.4 Hz), 52.35 (s, $N(CH_3)_2$), 47.07 (s, SCH_3, J_{CPt} = 63.9 Hz); ^{195}Pt NMR (86.18 MHz, $CDCl_3$): δ = −3657.92 (s); HRMS (ESI, pos. ion mode, CH_2Cl_2): *m/z* 507.1065 ($[M-Cl]^+$, calcd 507.1072); elementary analysis calcd for $C_{19}H_{22}ClNOPtS$: C, 42.03; H, 4.08; N, 2.58; S, 5.91; found: C, 42.15; H, 4.06; N, 2.62; S, 5.94.

2f: White solid; Yield: 61%; ^{1}H NMR (400 MHz, $CDCl_3$): δ = 8.84 (s, 1H, H^{10}, J_{HPt} = 48.0 Hz), 8.15–8.07 (m, 3H), 8.00–7.88 (m, 4H), 4.73 (s, 2H, CH_2N, J_{HPt} = 39.6 Hz), 3.66 (s, 6H, SCH_3, J_{HPt} = 20.8 Hz), 3.07 (s,

6H, $N(CH_3)_2$, $J_{HPt}=29.6$ Hz); $^{13}C\{^1H\}$ NMR (150.9 MHz, $CDCl_3$): $\delta=$ 139.43 (s, Q), 135.10 (s, Q), 131.53 (s, CH[10]), 131.35 (s, Q), 130.51 (s, Q), 130.09 (s, Q), 128.59 (s, *C*H), 127.71 (s, *C*H), 126.65 (s, *C*H), 125.57 (s, *C*H), 125.49 (s, Q), 125.17 (s, *C*H), 125.11 (s, Q), 124.72 (s, *C*H), 123.94 (s, *C*H), 123.12 (s, Q), 72.79 (s, CH_2N), 53.03 (s, $N(CH_3)_2$), 47.09 (s, SCH_3, $J_{CPt}=92.8$ Hz); ^{195}Pt NMR (86.18 MHz, $CDCl_3$): $\delta=$ −3632.35 (s). HRMS (ESI, pos. ion mode, CH_2Cl_2): *m/z* 531.1069 ($[M-Cl]^+$, calcd 531.1072); elemental analysis calcd for $C_{21}H_{22}ClNOPtS$: C, 44.48; H, 3.91; N, 2.47; S, 5.66; found: C, 44.53; H, 4.01; N, 2.51; S, 5.64.

RP-HPLC purity and stability analyses

The purity of each Pt^{II} complex was analyzed using the method in Table S1 in the Supporting Information (mobile phases of 0.1% formic acid in dH_2O and 0.1% formic acid in HPLC grade CH_3CN). For stability analyses, samples of each Pt^{II} complex were prepared in DMSO and diluted in dH_2O so that the final %DMSO was 0.4 before injection on the HPLC. Chromatograms were recorded at 280 nm.

X-ray crystal structure analysis

Single crystals suitable for X-ray diffraction analysis were obtained from the slow diffusion of hexane into a saturated solution of **2c** and **2f** in CH_2Cl_2/toluene/hexane (2:1:5) and CH_2Cl_2/hexane (1:3), respectively. A summary of crystal data collection and refinement parameters for all compounds are given in Tables S2-S4, S9-S11 in the Supporting Information. Crystals were mounted on glass fibres and transferred to the cold gas stream of the diffractometer Bruker Smart APEX. Data were recorded with Mo Kα radiation ($\lambda=$ 0.71073 Å) in ω scan mode. Absorption correction for the compound was based on multi-scans.

Both structures were solved by direct methods (SHELXS-97);[48] refinement was done by full-matrix least squares on F^2 using the SHELXL-97 program suite;[48] empirical (multi-scan) absorption correction with SADABS (Bruker).[49] Hydrogen atoms for aromatic CH, aliphatic CH, CH_2 and methyl groups were positioned geometrically (C–H = 0.95 Å for aromatic CH, C–H = 1.00 Å for aliphatic CH, C–H = 0.99 Å for CH_2, C–H = 0.98 Å for CH_3) and refined using a riding model (AFIX 43 for aromatic CH, AFIX 23 for CH_2, AFIX 137 for rotating group for CH_3), with $U_{iso}(H)=1.2U_{eq}(CH)$ and $U_{iso}(H)=1.5U_{eq}(CH_3)$. Graphics were drawn with DIAMOND (Version 3.2).[50] The structural data has been deposited with the Cambridge Crystallographic Data Center.[51]

Cell lines and culture conditions

Cell lines were obtained from American Tissue Culture Collection (ATCC, U.S.A.) or European Collection of Animal Cell Culture (ECACC, Salisbury, U.K.). The human melanoma cell line 518A2 was obtained from the Department of Radiotherapy, Medical University of Vienna (Austria). Breast cancer cells, MCF-7 and MDA-MB-231, as well as the non-tumorigenic EA.hy926 and BGM cells were grown in DMEM without phenol red that contains 1 g L^{-1} glucose supplemented with 10% (v/v) final concentration of heat-inactivated fetal bovine serum (FBS) (Sigma, USA), 2 mM L-glutamine, 2 mM sodium pyruvate, and antibiotics (penicillin/streptomycin) at 37 °C under a humidified atmosphere containing 7.5–10% CO_2. The 518A2 cell line was grown at 37 °C, 5% CO_2, 95% humidity in DMEM containing 10% FBS, 1% antibiotic-antimycotic, and 250 μg mL^{-1} gentamycin (all from Gibco). Human ovarian carcinoma A2780 and A2780cisR cell lines were grown in RPMI-1640, supplemented with 10% (v/v) final concentration of heat-inactivated FBS, 2 mM L-glutamine and antibiotics (penicillin/streptomycin) and maintained at 37 °C under a humidified atmosphere containing 5% CO_2. In all cases, cells from 80% confluent monolayers were removed from flasks using a 0.12% trypsin solution–0.05 mM EDTA (Sigma Aldrich), centrifuged at 200 *g* for 5 min and washed twice with PBS, and finally the cell pellet was diluted with complete medium. The medium was changed twice every week, and 1 μM CDDP was added to the A2780cisR cell line every two subcultures in order to retain resistance to CDDP. Before and after experiments, all cell lines were ensured to be mycoplasma-free, as determined by the Hoechst DNA stain method.[52] Flow cytometry experiments were carried out on a FACScalibur flow cytometer (Becton Dickinson & Co., Franklin Lakes, N). The in vitro studies were performed in the SACE service (Support Service for Experimental Sciences, University of Murcia, Murcia, Spain).

Cytotoxicity assays

Cell proliferation was evaluated by MTT assay. 5×10^3 cells were plated in 96-well sterile plates with 200 μL of medium and pre-incubated for 24 h. After attachment to the culture surface, cells were incubated with various concentrations of the compounds for 48 h at 37 °C. After the drug exposure, the medium was replaced by 200 μL of freshly medium and 50 μL of a MTT solution 5 mg mL^{-1} was added. Cells were left 4 h at 37 °C in the dark in these conditions. Finally, the solution of each plate was removed, 100 μL of DMSO was added and shook 5 min at 120 rpm. Absorbance was measured at 560 nm in a Fluorstar Omega spectrophotometer. The effects of complexes were expressed as corrected percentage inhibition values according to Equation (1)

$$\%\text{inhibition} = \left[1 - \left(\frac{T}{C}\right)\right] \times 100$$

where *T* is the mean absorbance of the treated cells and *C* the mean absorbance in the controls.

The inhibitory potential of compounds was measured by calculating concentration-percentage inhibition curves; these curves were adjusted to Equation (2)

$$E = \frac{E_{max}}{1 + \left(\frac{IC_{50}}{C}\right)^n}$$

where *E* is the percentage inhibition observed, E_{max} is the maximal effects, IC_{50} is the concentration that inhibits 50% of maximal growth, *C* is the concentration of compounds tested and *n* is the slope of the semi-logarithmic dose-response sigmoid curves. This non-linear fitting was performed using Sigma Plot 11.0 software.

All compounds were tested in three independent studies with quadruplicate points. The maximum % of DMSO used was 0.4 (except for CDDP, water diluted) and the measurements were corrected with a control containing the same amount of DMSO.

Apoptosis experiments

For apoptosis determination assays, 1.5×10^5 A2780 cells were seeded in a 6-well plate and incubated with compounds **2b**, **d,** or CDDP (1 μM) for 48 h. After treatment, cells were collected and washed twice with PBS as described above. Then, PBS was removed and 40 μL of a solution containing Annexin V and PI (Annexin-V-Fluos from Roche) and 160 μL of incubation buffer (10 mM hepes, 140 mM NaCl, 5 mM $CaCl_2$, pH 7.4) were added. Cells were resuspended in this solution and left at RT in the dark for 15 min. PBS (200 μL) was immediately added prior the measurements. In

each case, 10000 events were acquired and emissions were registered at 620 and 525 nm for PI and Annexin V, respectively, λ_{exc} = 488 nm.

Caspase-3 assay

Activation of Caspase-3 by compounds **2b**, **d,** and CDDP were determined in A2780 cells. In these experiments, 1×10^5 cells were plated in 6-well sterile plates with 2 mL of complete medium and pre-incubated overnight. Then, the compounds (1 μM) were added and allowed further incubation for 24 h. After treatment, cells were collected with Trypsin–EDTA and centrifuged at 200 *g* for 5 min. Cell pellet were resuspended in PBS (1 mL) and 1 μL of a FITC-DEVD-FMK solution (1 μL mL^{-1}) was added. Cells were incubated for 30 min at 37 °C in the dark. Finally, fluorescence was measured at λ_{em} = 535 nm with a flow cytometer, λ_{exc} = 488 nm. For each sample 10000 events were acquired.

Intracellular distribution in live cells by confocal microscopy

Intracellular distribution was performed in MCF-7 cells (5×10^4) in confocal culture dishes. Compound **2f** was added until a final concentration of 1 μM to the culture medium (final DMSO concentration, 0.1% v/v). After 1 h incubation at 37 °C, SYTO® 59 Red and Mitotracker® FM green were added at a final concentration of 500 and 200 nM, respectively. Cells were left in these conditions for 30 min. Then, cells were washed with phosphate free buffer (9% NaCl, 1 mL) and fluorescence was photographed with a Leica TCS SP2 confocal microscope (Leica Microsystems, Wetzlar, Germany) using a planapochromate 40×/NA 1.4 oil immersion objective. Image processing and display were carried out with ConfocalUniovi ImageJ. For high-resolution imaging, **2f**, SYTO, and Mitotracker were simultaneously excited with an internal air-cooled Argon and Neon ion lasers, λ_{exc} = 458, 488 and 633 nm.

Platinum cellular accumulation studies

Cellular accumulations of **2a**–**f** and CDDP were determined in A2780 human ovarian carcinoma cells. In these experiments, 1×10^6 A2780 cells were seeded on a 6-well culture plates. After overnight pre-incubation in drug-free medium at 37 °C in 5% CO_2 humidified atmosphere, the cells were treated with Pt^{II} complexes at 10 μM concentration and allowed further 3 h of drug exposure under similar conditions. After treatment, cells were harvested from the plate using Trypsin–EDTA and centrifuged at 200 *g* for 5 min, and the cell pellets were washed with 1 mL of PBS, were counted, transferred to Eppendorf tubes, and centrifuged at 10000 *g* for 5 min at 4 °C. The supernatant was discarded and the pellet was digested with 100 μL of sub-boiled HNO_3 (sub-bolied suprapur 65% nitric acid, Merck). Afterwards, quantity of metal taken up by the cells was determined by ICP-MS. All experiments were carried out in duplicate. As a control untreated cells were used.

Quantification of platinum bound to DNA

A2780 cells were seeded and treated with **2a**–**f** or CDDP as described above. For DNA isolation, the cell pellets were stored at −70 °C and after being lysed in DNAzol (DNAzol®, MRC) supplemented with RNAse A (100 mg mL^{-1}). Genomic DNA was precipitated from the lysate by 100% EtOH, washed twice with 75% EtOH and resuspended in 8 mM NaOH. The DNA content in each sample was determined by UV spectrophotometry (NanoDrop ND-1000). The amount of metal bound to DNA was quantified by ICP-MS. All measurements were done in duplicate.

EMSA Assay

Compounds **2b** and **d** were tested for their interaction with circular pBR322 plasmid DNA. 1.5 μg of plasmid DNA in TE-buffer (10 mM Tris-HCl, 1 mM EDTA, pH 8.0) was incubated with 0, 5, 10, 25, and 50 μM of **2b** or **d** for 24 h at 37 °C. An agarose gel electrophoresis (1% agarose in 0.5 TBE-buffer) was performed for 4 h at 66 V. The DNA was stained with ethidium bromide for 30 min and DNA bands were visualized with UV light. Results were confirmed by repetition of the experiment.

Intracellular reactive oxygen species (ROS) determination

Intracellular ROS were quantified to determine the oxidative stress in A2780 cell line after 24 h treatment with 1 μM **2b**, **d,** or CDDP. Cells (1×10^5 per well) were seeded on a 6-well plate and left attached overnight. The treated cells were harvested with Trypsin–EDTA and washed twice with PBS. Finally, pelleted cells were loaded with 25 μM DCFH-DA and incubated for 30 min at 37 °C. For each sample, 10000 events were acquired and emission was registered at 530 nm for DCF oxidation product with a flow cytometer, λ_{exc} = 488 nm. Untreated cells containing maximal concentration of DMSO used in the treatment (0.4%) were used as a control.

Mitochondrial polarization assay

Mitochondrial membrane potential was measured with the fluorescent probe Rho-123. Briefly, cells (1×10^5 per well) were seeded in 6-well plates and pre-incubated overnight. Then, compounds **2b**,**d**, or CDDP were added at a concentration of 1 μM and the cells were left to incubate for 24 h. After cells were collected and washed twice with PBS, Rho-123 (1 mM, Sigma Aldrich) was added to a final concentration of 1 μM. Samples were incubated for 15 min in these conditions. In all cases, 10000 events were analyzed with a flow cytometer λ_{exc} 488 and λ_{em} 530 nm, respectively.

Endothelial tube formation assay

Unpolymerized Matrigel (8.7 mg mL^{-1}; B&D Biosciences, Bedford, MA) was placed in 96-well plates (9 μL/well) and allowed to polymerize for 1 h at 37 °C. EA.hy926 cells (12×10^3 per well) were seeded on top of the Matrigel layer and incubated at 37 °C. This study revealed that tube formation was maximal after 12 h. Then, EA.hy926 cells were incubated at a final concentration of 1 μM of **2a**–**f** for 12 h. Afterwards, cells were photographed using an inverted phase-contrast microscope (Nikon mod. Eclipse TE-2000-U). Tube formation was quantified by measuring the total length of the tube, number of meshes, and area of meshes under 4× magnification using ImageJ software (National Institutes of Health, Bethesda, MD, USA).

CAM Assay

SPF-eggs (SPF = specific pathogen free) were incubated for 5 days at 37 °C and air humidity of 50–60%. On day 5, a hole was cut into the flat end of the eggs and the inner shell membrane was removed. The holes were resealed with Leukosilk® (Hansaplast) and the eggs were further incubated for 24 h. On day 6 of incubation, a silicone ring (5 and 6 mm, inner and outer diameter, respectively) was placed on the blood vessels of the CAM and the state of the CAM was documented using a Traveler microscope (0 h). After documentation 10 μL (5 or 10 nmol) of appropriate dilutions of pure DMSO or 10 mM stock solutions (in DMSO) of **2b** or **d** in H_2O were applied to the area enclosed by the silicone ring. Effects on the blood vessels of the CAM inside the ring caused by the com-

pounds were monitored after additional 6 h incubation with the applied substances. The experiments were conducted as triplicates for each complex and the DMSO negative control.

Tubulin polymerization

50 μL of Brinkley's buffer 80 (20% Glycerol and 3 mM of GTP) were pre-set in the wells of a 96-well μClear black-well half-area plate. Appropriate pre-dilutions of **2b** and **d** in H_2O from freshly dissolved solutions (10 mM in DMSO) were added to reach a working concentration of 20 μM. This was analogously done with DMSO as negative control and Combretastatin A4 as positive control. To each prepared well, tubulin was added (end concentration 5 $\mu g\,\mu L^{-1}$) and the OD was instantly measured at 340 nm using a pre-heated Tecan F200 plate reader. The results are representative for at least two repetitions of the assay.

Microtubules: tubulin staining

518A2-Melanoma cells were cultured on coverslips (12 mm in diameter) inside 24-well plates until they reached sub-confluency after 24 h ($0.05\times10^6\,mL^{-1}$) in DMEM. Appropriate dilutions of freshly prepared stock solutions of **2b** and **d** (in DMSO) were added to the cells so that the complexes reached a working concentration of 2 μM. Cells were further incubated for 24 h. For staining of tubulin cytoskeleton, the cells were washed with PBS and fixed in 3.7% formaldehyde solution (PBS). After washing with PBS, permeabilization and blocking (1% BSA, 0.1% Triton X-100 in BSA) of the cells was done and cells were incubated with a primary antibody against alpha-tubulin (anti-alpha-tubulin, monoclonal mouse antibody) for 1 h at 37 °C. After washing with PBS, cells were treated with the secondary goat anti-mouse Alexa Fluor® 488 antibody for 1 h at RT. The cells were washed twice with PBS and the coverslips were mounted in 4–88-based mounting medium containing 2.5% 1,4-diazabicyclo[2.2.2]octane (DABCO) and 1 $\mu g\,mL^{-1}$ 4′,6-diamidino-2-phenylindole (DAPI).

Statistical analysis

Analysis of variance test was used to comparison of quantitative variables between groups. All statistical analyses were performed using GraphPad Prism v.6. $*p<0.05$ and $*p<0.01$ were considered statically significant.

Acknowledgements

This work was supported by the Spanish Ministry of Economy and Competitiveness and FEDER funds (Project CTQ2015-64319-R; MINECO/FEDER, UE), and by Fundación Séneca-CARM (Project 15354/PI/10). COST Action CM1105 and MetDrugs network CTQ2015-70371-REDT (MINECO/FEDER, UE) for providing opportunities of discussion.

Conflict of interest

The authors declare no conflict of interest.

Keywords: angiogenesis · anticancer · antivascular · cyclometalated · platinum

[1] L. Kelland, *Nat. Rev. Cancer* **2007**, *7*, 573 – 584.
[2] a) D. Wang, S. J. Lippard, *Nat. Rev. Drug Discovery* **2005**, *4*, 307 – 320; b) G.-S. Oh, H.-J. Kim, A. Shen, S. B. Lee, D. Khadka, A. Pandit, H.-S. So, *Electrolyte Blood Pressure* **2014**, *12*, 55 – 65; c) S. Dasari, P. B. Tchounwou, *Eur. J. Pharmacol.* **2014**, *740*, 364 – 378.
[3] L. R. Kelland, *Drugs* **2000**, *59*, 1 – 8.
[4] a) L. Galluzzi, L. Senovilla, I. Vitale, J. Michels, I. Martins, O. Kepp, M. Castedo, G. Kroemer, *Oncogene* **2012**, *31*, 1869 – 1883; b) L. Galluzzi, I. Vitale, J. Michels, C. Brenner, G. Szabadkai, A. Harel-Bellan, M. Castedo, G. Kroemer, *Cell Death Dis.* **2014**, *5*, e1257.
[5] A. Bergamo, G. Sava, *Chem. Soc. Rev.* **2015**, *44*, 8818 – 8835.
[6] a) D. G. Teoh, A. A. Secord, *Cancer Control.* **2011**, *18*, 31 – 43; b) C. M. de Souza, A. C. Araújo e Silva, C. de Jesus Ferraciolli, G. V. Moreira, L. C. Campos, D. C. dos Reis, M. T. P. Lopes, M. A. N. D. Ferreira, S. P. Andrade, G. D. Cassali, *Biomed. Pharmacother.* **2014**, *68*, 51 – 57.
[7] a) C. M. Clavel, E. Păunescu, P. Nowak-Sliwinska, A. W. Griffioen, R. Scopelliti, P. J. Dyson, *J. Med. Chem.* **2015**, *58*, 3356 – 3365; b) V. Gandin, A. Trenti, M. Porchia, F. Tisato, M. Giorgetti, I. Zanusso, L. Trevisi, C. Marzano, *Metallomics* **2015**, *7*, 1497 – 1507; c) J. K. Muenzner, T. Rehm, B. Biersack, A. Casini, I. A. M. de Graaf, P. Worawutputtapong, A. Noor, R. Kempe, V. Brabec, J. Kasparkova, R. Schobert, *J. Med. Chem.* **2015**, *58*, 6283 – 6292; d) P. Nowak-Sliwinska, C. M. Clavel, E. Paunescu, M. T. te Winkel, A. W. Griffioen, P. J. Dyson, *Mol. Pharm.* **2015**, *12*, 3089 – 3096; e) E. Păunescu, P. Nowak-Sliwinska, C. M. Clavel, R. Scopelliti, A. W. Griffioen, P. J. Dyson, *ChemMedChem* **2015**, *10*, 1539 – 1547; f) J. K. Muenzner, B. Biersack, H. Kalie, I. C. Andronache, L. Kaps, D. Schuppan, F. Sasse, R. Schobert, *ChemMedChem* **2014**, *9*, 1195 – 1204; g) C. M. Clavel, E. Păunescu, P. Nowak-Sliwinska, A. W. Griffioen, R. Scopelliti, P. J. Dyson, *J. Med. Chem.* **2014**, *57*, 3546 – 3558; h) T. T.-H. Fong, C.-N. Lok, C. Y.-S. Chung, Y.-M. E. Fung, P.-K. Chow, P.-K. Wan, C.-M. Che, *Angew. Chem. Int. Ed.* **2016**, *55*, 11935 – 11939; *Angew. Chem.* **2016**, *128*, 12114 – 12118; i) J.-J. Zhang, J. K. Muenzner, M. A. Abu el Maaty, B. Karge, R. Schobert, S. Wolfl, I. Ott, *Dalton Trans.* **2016**, *45*, 13161 – 13168; j) J. Yellol, S. A. Pérez, A. Buceta, G. Yellol, A. Donaire, P. Szumlas, P. J. Bednarski, G. Makhloufi, C. Janiak, A. Espinosa, J. Ruiz, *J. Med. Chem.* **2015**, *58*, 7310 – 7327.
[8] J.-J. Zhang, R. W.-Y. Sun, C.-M. Che, *Chem. Commun.* **2012**, *48*, 3388 – 3390.
[9] C. Karnthaler-Benbakka, D. Groza, K. Kryeziu, V. Pichler, A. Roller, W. Berger, P. Heffeter, C. R. Kowol, *Angew. Chem. Int. Ed.* **2014**, *53*, 12930; *Angew. Chem.* **2014**, *126*, 13144.
[10] R. Schobert, B. Biersack, A. Dietrich, S. Knauer, M. Zoldakova, A. Fruehauf, T. Mueller, *J. Med. Chem.* **2009**, *52*, 241 – 246.
[11] C. Bincoletto, I. L. S. Tersariol, C. R. Oliveira, S. Dreher, D. M. Fausto, M. A. Soufen, F. D. Nascimento, A. C. F. Caires, *Bioorg. Med. Chem.* **2005**, *13*, 3047 – 3055.
[12] a) O. Pinato, C. Musetti, C. Sissi, *Metallomics* **2014**, *6*, 380 – 395; b) E. Meggers, *Chem. Commun.* **2009**, 1001 – 1010.
[13] M. V. Babak, S. M. Meier, K. V. M. Huber, J. Reynisson, A. A. Legin, M. A. Jakupec, A. Roller, A. Stukalov, M. Gridling, K. L. Bennett, J. Colinge, W. Berger, P. J. Dyson, G. Superti-Furga, B. K. Keppler, C. G. Hartinger, *Chem. Sci.* **2015**, *6*, 2449 – 2456.
[14] L. Di, E. H. Kerns, *Drug-like Properties: Concepts, Structure Design and Methods: from ADME to Toxicity Optimization*, Elsevier Science, Amsterdam, **2010**.
[15] J. A. Arnott, S. L. Planey, *Expert Opin. Drug Discovery* **2012**, *7*, 863 – 875.
[16] a) H. Chen, J. A. Parkinson, R. E. Morris, P. J. Sadler, *J. Am. Chem. Soc.* **2003**, *125*, 173 – 186; b) Z. Liu, A. Habtemariam, A. M. Pizarro, G. J. Clarkson, P. J. Sadler, *Organometallics* **2011**, *30*, 4702 – 4710; c) Z. Liu, A. Habtemariam, A. M. Pizarro, S. A. Fletcher, A. Kisova, O. Vrana, L. Salassa, P. C. A. Bruijnincx, G. J. Clarkson, V. Brabec, P. J. Sadler, *J. Med. Chem.* **2011**, *54*, 3011 – 3026; d) S. H. van Rijt, A. Mukherjee, A. M. Pizarro, P. J. Sadler, *J. Med. Chem.* **2010**, *53*, 840 – 849; e) M. J. Chow, M. V. Babak, D. Y. Q. Wong, G. Pastorin, C. Gaiddon, W. H. Ang, *Mol. Pharm.* **2016**, *13*, 2543 – 2554.
[17] a) V. Pichler, P. Heffeter, S. M. Valiahdi, C. R. Kowol, A. Egger, W. Berger, M. A. Jakupec, M. Galanski, B. K. Keppler, *J. Med. Chem.* **2012**, *55*, 11052 – 11061; b) P. Gramatica, E. Papa, M. Luini, E. Monti, M. B. Gariboldi, M. Ravera, E. Gabano, L. Gaviglio, D. Osella, *J. Biol. Inorg. Chem.* **2010**, *15*, 1157 – 1169.
[18] M.-G. Mendoza-Ferri, C. G. Hartinger, R. E. Eichinger, N. Stolyarova, K. Severin, M. A. Jakupec, A. A. Nazarov, B. K. Keppler, *Organometallics* **2008**, *27*, 2405 – 2407.

[19] A. J. Millett, A. Habtemariam, I. Romero-Canelón, G. J. Clarkson, P. J. Sadler, *Organometallics* **2015**, *34*, 2683 – 2694.
[20] a) J. Ruiz, V. Rodríguez, N. Cutillas, A. Espinosa, M. J. Hannon, *Inorg. Chem.* **2011**, *50*, 9164 – 9171; b) J. Ruiz, V. Rodríguez, N. Cutillas, A. Espinosa, M. J. Hannon, *J. Inorg. Biochem.* **2011**, *105*, 525 – 531.
[21] A. Zamora, S. A. Pérez, V. Rodríguez, C. Janiak, G. S. Yellol, J. Ruiz, *J. Med. Chem.* **2015**, *58*, 1320 – 1336.
[22] T. S. De Vries, A. Prokofjevs, J. N. Harvey, E. Vedejs, *J. Am. Chem. Soc.* **2009**, *131*, 14679 – 14687.
[23] a) S. Bhattacharyya, *J. Org. Chem.* **1995**, *60*, 4928 – 4929; b) G. Cai, Y. Fu, Y. Li, X. Wan, Z. Shi, *J. Am. Chem. Soc.* **2007**, *129*, 7666 – 7673.
[24] C. H. M. Amijs, G. P. M. van Klink, M. Lutz, A. L. Spek, G. van Koten, *Organometallics* **2005**, *24*, 2944 – 2958.
[25] J. Ruiz, J. Lorenzo, C. Vicente, G. López, J. M. López-de-Luzuriaga, M. Monge, F. X. Avilés, D. Bautista, V. Moreno, A. Laguna, *Inorg. Chem.* **2008**, *47*, 6990 – 7001.
[26] G. R. Desiraju, T. Steiner, *The weak hydrogen bond, in: IUCr Monograph on Crystallography, Vol. 9*, Oxford Science, Oxford, **1999**.
[27] a) H. A. Habib, A. Hoffmann, H. A. Höppe, G. Steinfeld, C. Janiak, *Inorg. Chem.* **2009**, *48*, 2166 – 2180; b) B. Wisser, C. Janiak, *Z. Anorg. Allg. Chem.* **2007**, *633*, 1796 – 1800.
[28] a) M. Nishio, *Phys. Chem. Chem. Phys.* **2011**, *13*, 13873 – 13900; b) M. Nishio, Y. Umezawa, K. Honda, S. Tsuboyama, H. Suezawa, *CrystEngComm* **2009**, *11*, 1757 – 1788; c) M. Nishio, *CrystEngComm* **2004**, *6*, 130 – 158; d) C. Janiak, S. Temizdemir, S. Dechert, W. Deck, F. Girgsdies, J. Heinze, M. J. Kolm, Tobias G. Scharmann, O. M. Zipffel, *Eur. J. Inorg. Chem.* **2000**, 1229 – 1241; e) Y. Umezawa, S. Tsuboyama, K. Honda, J. Uzawa, M. Nishio, *Bull. Chem. Soc. Jpn.* **1998**, *71*, 1207 – 1213; f) M. Nishio, M. Hirota, Y. Umezawa, *The CH/π interaction (evidence, nature and consequences)*, Wiley-VCH, New York, **1998**.
[29] a) X.-J. Yang, F. Drepper, B. Wu, W.-H. Sun, W. Haehnel, C. Janiak, *Dalton Trans.* **2005**, 256 – 267; b) C. Janiak, *J. Chem. Soc. Dalton Trans.* **2000**, 3885 – 3896.
[30] L. R. Kelland, C. F. Barnard, K. J. Mellish, M. Jones, P. M. Goddard, M. Valenti, A. Bryant, B. A. Murrer, K. R. Harrap, *Cancer Res.* **1994**, *54*, 5618 – 5622.
[31] G. S. Salvesen, S. J. Riedl, in *Programmed Cell Death in Cancer Progression and Therapy*, Springer Netherlands, Dordrecht, **2008**, pp. 13 – 23.
[32] a) K. Valkó, *J. Chromatogr. A* **2004**, *1037*, 299 – 310; b) A. I. Fernández-Llamazares, J. Adan, F. Mitjans, J. Spengler, F. Albericio, *Bioconjugate Chem.* **2014**, *25*, 11 – 17.
[33] a) V. Novohradsky, Z. Liu, M. Vojtiskova, P. J. Sadler, V. Brabec, J. Kasparkova, *Metallomics* **2014**, *6*, 682 – 690; b) M. Hanif, A. A. Nazarov, C. G. Hartinger, W. Kandioller, M. A. Jakupec, V. B. Arion, P. J. Dyson, B. K. Keppler, *Dalton Trans.* **2010**, *39*, 7345 – 7352.
[34] a) S. P. Oldfield, M. D. Hall, J. A. Platts, *J. Med. Chem.* **2007**, *50*, 5227 – 5237; b) M. M. Hann, G. M. Keserü, *Nat. Rev. Drug Discovery* **2012**, *11*, 355 – 365; c) R. J. Young, D. V. S. Green, C. N. Luscombe, A. P. Hill, *Drug Discovery Today* **2011**, *16*, 822 – 830.
[35] Y. Hiraoka, T. Shimi, T. Haraguchi, *Cell Struct. Funct.* **2002**, *27*, 367 – 374.
[36] G. Y. Park, J. J. Wilson, Y. Song, S. J. Lippard, *Proc. Natl. Acad. Sci. USA* **2012**, *109*, 11987 – 11992.
[37] S. Imstepf, V. Pierroz, P. Raposinho, M. Bauwens, M. Felber, T. Fox, A. B. Shapiro, R. Freudenberg, C. Fernandes, S. Gama, G. Gasser, F. Motthagy, I. R. Santos, R. Alberto, *Bioconjugate Chem.* **2015**, *26*, 2397 – 2407.
[38] a) V. Pichler, S. Goschl, E. Schreiber-Brynzak, M. A. Jakupec, M. Galanski, B. K. Keppler, *Metallomics* **2015**, *7*, 1078 – 1090; b) V. Novohradsky, L. Zerzankova, J. Stepankova, A. Kisova, H. Kostrhunova, Z. Liu, P. J. Sadler, J. Kasparkova, V. Brabec, *Metallomics* **2014**, *6*, 1491 – 1501; c) W. Kandioller, E. Balsano, S. M. Meier, U. Jungwirth, S. Goschl, A. Roller, M. A. Jakupec, W. Berger, B. K. Keppler, C. G. Hartinger, *Chem. Commun.* **2013**, *49*, 3348 – 3350; d) F. Cisnetti, A. Gautier, *Angew. Chem. Int. Ed.* **2013**, *52*, 11976 – 11978; *Angew. Chem.* **2013**, *125*, 12194 – 12196.
[39] M. Schmidlehner, L. S. Flocke, A. Roller, M. Hejl, M. A. Jakupec, W. Kandioller, B. K. Keppler, *Dalton Trans.* **2016**, *45*, 724 – 733.
[40] a) D. Trachootham, J. Alexandre, P. Huang, *Nat. Rev. Drug Discovery* **2009**, *8*, 579 – 591; b) S. Wen, D. Zhu, P. Huang, *Future Med. Chem.* **2013**, *5*, 53 – 67.
[41] K. H. Kim, J. Y. Park, H. J. Jung, H. J. Kwon, *Biochem. Biophys. Res. Commun.* **2011**, *404*, 541 – 545.
[42] E. I. Deryugina, J. P. Quigley, *Histochem. Cell Biol.* **2008**, *130*, 1119 – 1130.
[43] D. W. Siemann, *Cancer Treat. Rev.* **2011**, *37*, 63 – 74.
[44] G. C. Tron, T. Pirali, G. Sorba, F. Pagliai, S. Busacca, A. A. Genazzani, *J. Med. Chem.* **2006**, *49*, 3033 – 3044.
[45] J. H. Price, A. N. Williamson, R. F. Schramm, B. B. Wayland, *Inorg. Chem.* **1972**, *11*, 1280 – 1284.
[46] M. D. Meijer, A. W. Kleij, B. S. Williams, D. Ellis, M. Lutz, A. L. Spek, G. P. M. van Klink, G. van Koten, *Organometallics* **2002**, *21*, 264 – 271.
[47] P. G. Young, K. Hirose, Y. Tobe, *J. Am. Chem. Soc.* **2014**, *136*, 7899 – 7906.
[48] G. M. Sheldrick, *Acta Crystallogr. Sect. A* **2008**, *64*, 112 – 122.
[49] G. M. Sheldrick, Program SADABS, University of Göttingen, Göttingen, Germany (**1996**).
[50] B. DIAMOND 3.2 for Windows. Crystal Impact Gbr, Germany; http://www.crystalimpact.com/diamond.
[51] CCDC 1508163 (**2 f**), and 1508164 (**2 c**) contain the supplementary crystallographic data for this paper. These data are provided free of charge by The Cambridge Crystallographic Data Centre.
[52] T. R. Chen, *TCA Manual* **1976**, *1*, 229 – 232.

Manuscript received: February 15, 2017
Accepted Article published: March 9, 2017
Final Article published: March 30, 2017